A Mathematical Model for the AC Impedance of Semiconducting Electrodes

A mathematical model is developed to calculate the impedance response of a semiconductor electrode to a sinusoidal current perturbation. The model accounts explicitly for electron and hole transport as well as generation and recombination through band-to-band mechanisms and through bulk interband electron acceptors of specified energy. The resistive (real) component of the impedance is shown to be sensitive to the concentration, distribution, and energy level of the bulk sites. The capacitive (imaginary) component, while useful for determining the dopant level and the flat-band potential of the semiconductor, is relatively insensitive to low concentrations of bulk sites.

D. B. Bonham, M. E. Orazem
Department of Chemical Engineering
University of Virginia
Charlottesville, VA 22901

Introduction

Surface and bulk electronic states have a significant impact on the performance of electronic devices. The need to control these species has prompted the development and use of several techniques to identify and measure the concentrations of specific states. Since many of the analytic tools available for this purpose (e.g., Auger spectroscopy and SIMS) are destructive and require the use of a vacuum chamber, there has been recent interest in the development of simple, sensitive, and nondestructive techniques. Impedance techniques have become popular for this application because they are nondestructive and are sensitive to electronic states that would also influence the performance of electronic devices. The data from impedance methods are currently interpreted through use of analytic kinetic models or analog equivalent circuits. Unfortunately, the impedance response of semiconductors is complex and often cannot be described analytically without restrictive assumptions. In order to eliminate the need for these assumptions, a mathematical model was developed that predicts the influence of deep-level bulk electronic states for an ideally polarizable n-GaAs semiconductor electrode. This treatment is sufficiently general that it would apply to other semiconducting materials with the appropriate changes in physical properties.

Bulk interband states can arise from a number of sources, including atomic impurities substituted into the semiconductor lattice, vacancies arising from missing lattice elements, interstitial states, and dislocation states from faults in the lattice geometry. These states arise from the conditions of crystal growth, which are, incidentally, more impure than those for silicon. Ghandhi (1983) presents a summary for the energy levels of a number of deep-level impurities in GaAs, given in Table 1. Certain bulk states are intentionally introduced (e.g., shallow-level species are introduced to be n- and p-type dopants, and chromium is used to form semiinsulating GaAs), while others are undesirable (e.g., highly mobile oxygen in GaAs). Surface states, unlike bulk states, are often the product of their post-growth environment. For example, GaAs has been shown to have no intrinsic surface states in vacuum, but adsorbed metals and oxygen are known to form interband electronic states on GaAs. Surface states can also arise due to corrosion products and surface pretreatment.

Electrical characteristics resulting from the addition of surface or bulk states depend on whether these states are donor- or acceptorlike in nature. Donor species are those that become positively charged when an electron is released, while acceptors become negatively charged when an electron is added. Because these species are charged, the distribution of electrical potential can be affected. The treatment presented here is for electron acceptors distributed within the bulk of a semiconductor, such as chromium in GaAs.

Studies of semiconductor/electrolyte systems typically depend on *in situ* AC impedance techniques since the properties of these systems depend on the nature of the interface. However, these techniques are also used to study solid-state components because the electrolyte or liquid mercury used to provide the necessary electrical contact can be both nondestructive and easily removed. A variety of techniques based on AC impedance have been developed to study semiconductors. For example, Haak et al. (1982, 1984) and Haak and Tench (1984a, b) describe the use of electrochemical photocapacitance spectros-

Table 1. Ionization Energies for Deep-Level Species in GaAs*

Impurity	Type	Donor Level, from E_c eV	Acceptor Level, from E_v eV
O	n	0.40, 0.75	—
Co	p	—	0.16, 0.56
Cu	p	—	0.14, 0.24, 0.44
Cr	p	—	0.79
Fe	p	—	0.38, 0.52
Ni	p	—	0.35, 0.42
Au	p	—	0.09
Ag	p	—	0.11

*Ghandi (1983)

copy in which the capacity of a reverse-biased electrode is measured as a function of the wavelength of incident sub-bandgap light. Heller et al. (1978) discuss two-beam photocurrent spectroscopy used for semiconducting electrodes where a chopped light beam of a given frequency is superimposed on a constant-intensity beam of another frequency. Modulation of the illumination intensity has also been used in single-beam photocurrent techniques (Kamieniecki, 1983). Capacitance-voltage data are commonly used to identify the flat-band potential and the doping level for semiconductors (Nicollian and Goetzberger, 1967; DeClerck et al., 1973; Tomkiewicz, 1979). At low frequencies, the conductive component of the AC response is more sensitive to mid-bandgap electronic states than is the capacitive component. The work of Nicollian and Goetzberger, DeClerck et al., and Nagasubramanian et al. (1983) emphasized variations in the conductive component and attributed these variations to mid-bandgap surface states. Wheeler et al. (1984) discuss the use of second harmonic AC impedance and differential photocurrent techniques. Related technqiues involve the use of electroluminescence, photoluminescence, and sub-bandgap photoresponse (Ghosh et al., 1969; Pettinger et al., 1976; Morisaki and Yazawa, 1978; Nakato et al., 1982; Butler and Ginley, 1983).

Previous modeling work

Development of mathematical models for the impedance response of semiconducting systems generally takes place in two steps: development of a steady state model followed by development of a model treating the sinusoidal perturbation of voltage or current about the steady state values. Some models that treat the influence of surface or bulk mid-bandgap electronic states are discussed below.

Steady State Models. Both analytic and numerical models have been developed for the steady state behavior of semiconductor systems. Orazem and Newman (1986) provide a review of analytic and numerical models. Most of these provide extensions to a model described by Gärtner (1959) for a reverse-biased p-n semiconductor junction. This model allows calculation of current density based on a drift component for carriers generated inside the depletion region and a diffusion component due to minority carriers generated outside this region. Major constraints are that recombination of carriers must be negligible in the space charge region (no bulk sites) and that the electrochemical potential (quasi-Fermi level) must be constant throughout the phase. Recent surface-state models have improved upon the Gärtner model by using kinetic expressions for steady state trapping and by calculating changes in the Helmholtz layer (Kelly and Memming, 1982; Li and Peter, 1985; and Kobayashi et al., 1985). The same restrictions of the Gärtner expression still apply, however, and these restrictions prohibit treatment of bulk mid-bandgap electronic states. While analytic expressions have been developed that circumvent these restrictions (McCann and Hanneman, 1982), complete treatment requires the use of numerical methods.

One-dimensional steady state numerical studies have been presented by Orazem and Newman (1984a, b) Orazem (1987), and Schwartz et al. (1985). These models circumvent the restrictions necessary for the analytic solutions described above. Bulk and surface recombination reactions were included, but none of these models allowed for changes in potential distribution due to trap-site charging; see Eq. 3. The influence of electrolytic mass transfer limitations was examined by Orazem (1987) for charge transfer between the electrolyte and valence band, conduction band, or surface states. The work by Schwartz et al. was intended for solid-state applications and included Auger recombination terms for very high light intensities. Laser and Bard (1976a, b) present the results of steady and unsteady state numerical models for the semiconductor electrode which do not treat explicitly the transport in the electrolyte. Their work illustrates the difficulty encountered in treating the coupling between the space-charge and electrically neutral regions of the semiconductor in that convergence was obtained only for thicknesses equal to the space-charge region thickness.

Steady state data are usually presented in the form of current-potential (I-V) curves. While surface and bulk states influence the shapes of these curves, these changes can be subtle, and it is difficult to obtain quantitative information concerning electronic states from steady state data.

Impedance Models. The impedance response of a semiconducting electrode and other electrochemical systems follows that expected for electrical circuits composed of combinations of capacitors, resistors, and inductors. For this reason, these systems are typically modeled through the use of equivalent electrical circuits. A specific circuit is deemed to provide a good model if the component values, obtained by nonlinear regression of the data, are independent of frequency. The component values can be expressed in terms of kinetic and transport properties by comparing the impedance obtained for an analytic model to the impedance response of the equivalent circuit. This approach provides a physical interpretation for values for the solid-state electrical components. The component values, however, generally depend on applied potential, and this complicates the interpretation of experimental results. Unfortunately, the analytic models that are used to extract this information require approximations that may restrict the conditions under which these techniques are valid. Elimination of these restrictions requires solution of highly coupled equations that must be solved by numerical techniques.

Dare-Edwards et al. (1983), Kobayashi et al. (1985), Li and Peter (1985), and Allongue and Cachet (1985) have developed and applied analytic impedance techniques based on perturbations to the steady state expressions discussed above. Due to the sequential nature of their development, any restrictions applicable to a steady state model are inherited by the impedance model. Fairly complete expressions have been developed for ideally polarizable unilluminated semiconductor electrodes that account for the influence of surface states. Dare-Edwards et al.

obtained electrical circuit component values in terms of interfacial and bulk semiconductor parameters by comparing solutions obtained through solution of transport and kinetic expressions appropriate for an equilibrated unilluminated semiconductor with those for a suggested equivalent circuits (see also Kobayashi et al., 1985. Analytic treatment of the effect of illumination or bulk states requires more restrictive assumptions.

Impedance behavior for ideally polarizable (complete blocking) semiconductor electrodes under dark conditions was modeled extensively by McDonald (1953, 1958). The procedure outlined in his work is quite general and has the same basis as the techniques used in this work.

Theoretical Development

The purpose of this work was to predict the effect of bulk states on the AC impedance of a semiconductor electrode. This work describes the sinusoidal steady state behavior of a system previously treated in the steady state by Orazem and Newman (1984a, b). This work also provides an extension of the work of McDonald (1953, 1958) by treating the transport of both majority and minority carriers with different values of diffusion coefficients and by treating generation and recombination through deep-level electronic states as well as through band-to-band mechanisms.

The equations that govern the semiconductor electrode apply to both steady and unsteady conditions. The electrostatic potential and the concentrations of electrons, holes, and ionized mid-bandgap acceptor states are dependent variables for this system. The shallow-level doping species were assumed to be completely ionized, as is appropriate at room temperatures. The general form for the material balance for any of the electronic species is given as (Newman, 1973)

$$\frac{\partial c_i}{\partial t} = \frac{\partial N_{yi}}{\partial y} + R_i \tag{1}$$

where

$$N_{yi} = -z_i c_i u_i F \frac{\partial \Phi}{\partial y} - D_i \frac{\partial c_i}{\partial y} \tag{2}$$

The flux of electrons and holes is therefore driven by concentration and potential gradients. The mid-bandgap acceptor species were assumed to be immobile; therefore, the rate of change of concentration was equal to the net time-dependent rate of production of ionized species. Poisson's equation,

$$\frac{\partial^2 \Phi}{\partial y^2} = -\frac{F}{\epsilon_{sc}}\{p - n + N_d - N_a\} \tag{3}$$

was used to relate the potential to the charge held within the semiconductor. In contrast to Orazem and Newman (1984a), the term $(N_d - N_a)$ was taken here to include the charge associated with ionized mid-bandgap acceptors as well as the ionized dopant species.

The reactions through various electronic states treated here are presented in Figure 1. As this work applies only to dark conditions, electrons gain energy to move to higher energy levels only through thermal excitation. The approach taken here can, of course, be easily extended to treat the AC impedance of illuminated semiconductors by incorporating photoexcitation of electrons into the steady state solution. A unique aspect of this work was that the rate and equilibrium constants for homogeneous recombination through trap sites were written explicitly in terms of the energy differences between the valence band, the traps, and the conduction band. This combination of kinetic and energetic viewpoints allows us to show explicitly the effect of varying the energy level of the acceptor species. For example, the material balance for the acceptor species was written as (Grove, 1967)

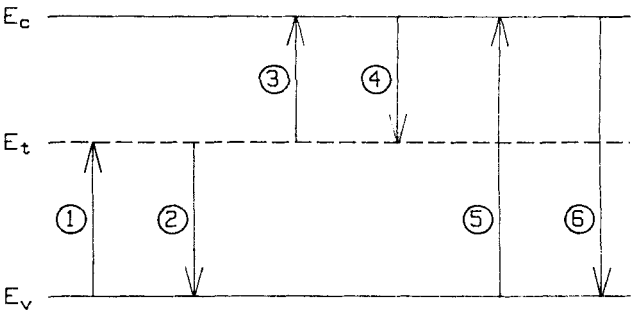

Figure 1. Energy levels associated with electronic transitions.

$$\frac{dc_{A^-}}{dt} = -k_2[pc_{A^-} - E_{12}(c_A - c_{A^-})] - k_4[E_{34}c_{A^-} - n(c_A - c_{A^-})] \tag{4}$$

where the equilibrium constant for reactions 1 and 2 represented in Figure 1 was related to electronic energy levels by

$$E_{12} = \frac{k_1}{k_2} = N_v g \exp[(E_v - E_t)/kT] \tag{5a}$$

and the corresponding term for reactions 3 and 4 was given by

$$E_{34} = \frac{k_3}{k_4} = \frac{N_c}{g} \exp[(E_t - E_c)/kT] \tag{5b}$$

where g is the degeneracy associated with the trap site. These expressions were derived by assuming thermal equilibrium and substituting standard expressions for ionized acceptor concentration in terms of energy level. The numerical value for this parameter is determined by the electronic character of the state; for example, $g = 4$ for electron acceptors, and $g = 2$ for electron donors (Sze, 1969). The parameter variation studies were simplified by the assumption that the rate constants were also interrelated such that, given energy levels for the electronic states, all rate constants could be obtained from one single value. For example, (Orazem and Newman, 1984a),

$$k_4 = k_2\left(\frac{E_{12}}{E_{34}}\right)^{1/2} \tag{6a}$$

This result was obtained by assuming that changes in the free energy of reaction associated with varying the energy of an elec-

tronic state are distributed equally between the activation energies for the forward and reverse directions. The approach taken here is similar to the standard approach used to separate the free energy of an electrochemical reaction into chemical and electrical terms. The symmetry factor in this application is assumed to have a value of ½ (Newman, 1973). Similar expressions were developed for band-to-band recombination, that is,

$$k_2 = k_6 \left(\frac{E_{56}}{E_{12}}\right)^{1/2} \tag{6b}$$

The use of Eq. 6b to relate the homogeneous, band-to-band rate constant k_6 to the corresponding interband constants k_2 (and k_4) is equivalent to assuming that the reaction cross section is the same for recombination through trap sites as it is for direct band-to-band recombination. This assumption could easily be relaxed to account for enhanced rates of recombination through trap sites.

Within this analysis, the dependent variables were separated into components that represent their steady state values and a perturbation from steady state caused by the superimposed current (McDonald, 1953). Thus, the current was given by

$$i = \bar{i} + \tilde{i}_r \exp(j\omega t) \tag{7a}$$

the concentration of electrons by

$$n = \bar{n} + (\tilde{n}_r + j\tilde{n}_j) \exp(j\omega t) \tag{7b}$$

the concentration of holes by

$$p = \bar{p} + (\tilde{p}_r + j\tilde{p}_j) \exp(j\omega t) \tag{7c}$$

the electrical potential by

$$\Phi = \bar{\Phi} + (\tilde{\Phi}_r + j\tilde{\Phi}_j) \exp(j\omega t) \tag{7d}$$

and the concentration of ionized electron acceptors by

$$c_{A^-} = \bar{c}_{A^-} + (\tilde{c}_{A^-,r} + j\tilde{c}_{A^-,j}) \exp(j\omega t) \tag{7e}$$

In the above equations, an overbar represents the steady state value, and a tilde represents the perturbation value. The actual concentration or potential at a given point in time and space would be given by the real part of the expressions given above. A similar approach has been taken to model the AC impedance of electrochemical systems (Tribollet and Newman, 1984; Cheng and Chin, 1984a, b, 1985).

The steady state equations were solved subject to the boundary conditions

$$\bar{N}_p = 0, \qquad \frac{d\bar{\Phi}}{dy} = 0$$

and

$$\bar{i} = 0$$

at the semiconductor-current collector interface, and

$$\bar{N}_n = 0, \qquad \bar{\Phi} = 0$$

and

$$\frac{d\bar{\Phi}}{dy} = -\frac{q_{sc}}{\epsilon_{sc}}$$

at the semiconductor-electrolyte interface. These conditions are appropriate for a perfect ohmic contact and an ideally polarized semiconductor-electrolyte or semiconductor-mercury interface, respectively. These equations were linearized, written in finite-difference form, and solved using the BAND algorithm developed by Newman (1968) coupled with Newton-Raphson iteration. This method for solution of the governing equations requires no linearization approximations and avoids assumptions involving depletion or neutral zones.

The time-dependent equations were solved for the response to a superimposed sinusoidal current by introducing Eqs. 7a–7e into the governing Eqs. 1–6 and linearizing around the steady state solution obtained in the previous step. The resulting set of linear ordinary differential equations was also solved with the BAND algorithm, and an iterative technique was used to minimize round-off errors. The boundary conditions for the impedance calculations were given by

$$\tilde{N}_{p,j} = \tilde{N}_{p,r} = 0$$

$$\tilde{p}_j = \tilde{p}_r = 0$$

and

$$\tilde{n}_j = \tilde{n}_r = 0$$

at the semiconductor-current-collector interface, and by

$$\tilde{N}_{n,j} = \tilde{N}_{n,r} = 0$$

$$\tilde{\Phi}_j = \tilde{\Phi}_r = 0$$

$$\frac{d\tilde{\Phi}_j}{dy} = \frac{\tilde{i}_r}{\epsilon_{sc}\omega}$$

and

$$\frac{d\tilde{\Phi}_r}{dy} = 0$$

at the semiconductor-electrolyte interface. These conditions are consistent with an ideally polarized electrode where the superimposed current acts only as a charging current.

The calculated impedance

$$Z = Z_r + jZ_j \tag{8a}$$

has real and imaginary components given by

$$Z_r = \frac{\Delta\tilde{\Phi}_r}{\tilde{i}_r} \tag{8b}$$

and

$$Z_j = \frac{\Delta\tilde{\Phi}_j}{\tilde{i}_r} \tag{8c}$$

respectively.

Table 2. Dependent Variables

	Steady State
$\bar{\Phi}$	Potential
$\bar{n}$	Electron concentration
$\bar{p}$	Hole concentration
$\bar{c}_{A^-}$	Ionized trap concentration
	Sinusoidal Steady State
$\tilde{\Phi}_r, \tilde{\Phi}_j$	Potential
$\tilde{n}_r, \tilde{n}_j$	Electron concentration
$\tilde{p}_r, \tilde{p}_j$	Hole concentration
$\tilde{c}_{A^-,r}, \tilde{c}_{A^-,j}$	Ionized trap concentration

A summary of dependent variables for the steady state and sinusoidal steady state calculations is given in Table 2, and a list of parameter values is given in Table 3.

The system modeled in this work was uniformly doped n-GaAs under ideally polarized conditions. The applied potential changes the charge held within the semiconductor, and this changes the degree of band-bending. Completely filled or empty electronic states do not contribute to the real impedance response, and the extent to which trap states are filled depends on the local potential. Variation of band-bending in the semiconductor can therefore be used as a probe to sample the local effects of the trap states, and the required variations of band-bending can be obtained experimentally through a properly chosen electrolyte or mercury contact. The mathematical model developed above incorporates critical experimental parameters, such as applied voltage and the frequency at which the impedance is determined, in addition to physical properties, such as trap energy level and diffusion coefficients, that can be independently measured. The linearization of the time-dependent expressions with a first-order Taylor series expansion about the steady state requires that the perturbations be small when compared to the steady state values. This treatment is exactly analogous to experimental impedance studies which require that the amplitude of the perturbation be sufficiently large to create an acceptable signal-to-noise ratio, yet be small enough to allow simplified treatment of the data.

Results and Discussion

A calculated Mott-Schottky representation for an n-type GaAs semiconductor with a nonuniform trap state distribution is presented in Figure 2. The trap energy was assumed to be 1.0 eV referenced to the valence band energy, and these states were

Table 3. Parameter Values

E_g	Band gap*	1.43	eV
n_i	Intrinsic concentration*	1.1×10^7	cm^{-3}
		(1.83×10^{-11})	equiv./m^3)
$N_d - N_a$	Dopant concentration	1×10^{16}	cm^{-3}
		(1.66×10^{-2})	equiv./m^3)
D_{e^-}	Electron diffusivity*	145	cm^2/s
		$(1.45 \times 10^{-2}$	$m^2/s)$
D_{h^+}	Hole diffusivity*	8.28	cm^2/s
		$(8.28 \times 10^{-4}$	$m^2/s)$
ϵ_{sc}	Permittivity*	9.65×10^{-13}	C/V cm
		$(9.65 \times 10^{-11}$	C/V m)
k_5	Homogeneous recombination rate constant**	6.02×10^8	$m^3/mol \cdot s$

*Sze (1969)
**Adapted from Fahrenbruch and Bube (1983)

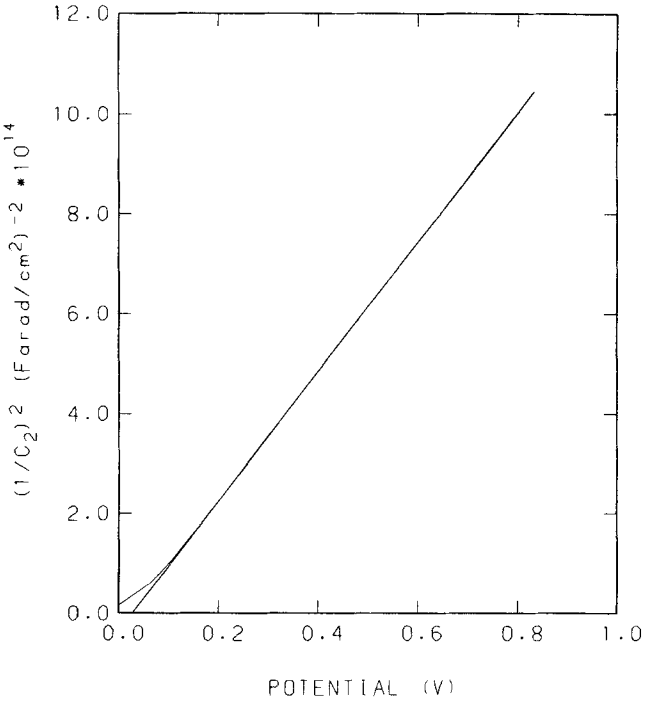

Figure 2. Mott-Schottky plot for a nonuniform distribution of trap states with energy 1.0 eV referenced to valence band.

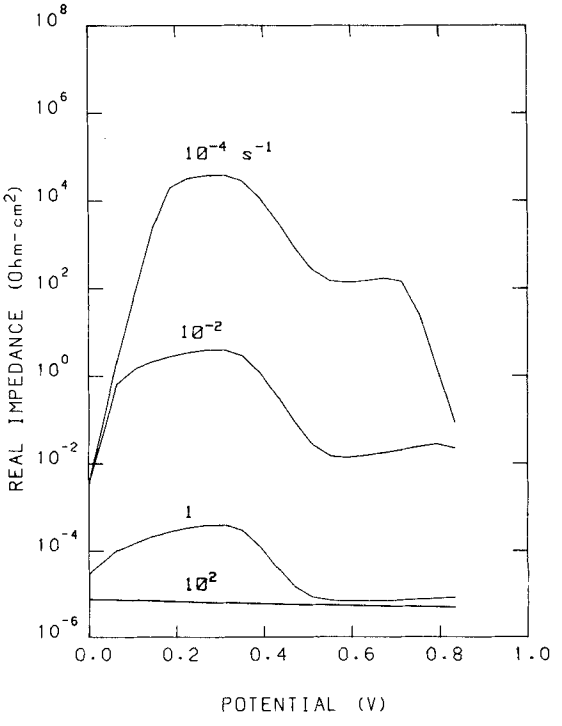

Figure 3. Real part of impedance as a function of applied potential (referenced to flat-band potential) with frequency as a parameter.
Trap energy and distribution as in Figure 2

distributed according to $\bar{c}_{A^-} = c^o_{A^-} \exp(-\alpha y/\lambda)$, where $c^o_{A^-}$ was equal to 10^{13} cm^{-3}, and α was equal to 29.95. This caused the distribution to decrease by a factor of 200 within a distance equal to one Debye length λ. This plot was shown to be independent of frequency over a range of 10^6 to 10^{-4} s^{-1}, which is approximately the maximum operating range of modern electronic instrumentation for AC impedance. In this case the capacity, obtained under the assumption that the calculated impedance data can be represented by a capacitor and resistor in series (i.e., $C = j/\omega Z_j$), was independent of frequency. The potential calculated here is referenced to the flat-band potential, defined to be the applied potential required for a uniform potential distribution in the semiconductor. The superimposed straight line is the commonly used Mott-Schottky equation. The slope of this line is proportional to the doping level, and the intercept at infinite capacity is shifted from flat band by a factor of kT.

The capacitance calculated above was insensitive to trap species altogether. This is because the dominant capacitance is due to the space charge region, which is related to the total concentration of charged species. The ionized trap densities used in this analysis were at most 0.1% of the doping density. In contrast, the real part of the impedance was sensitive to trap states at some frequencies, as shown in Figure 3. The asymptotic behavior at high frequency is that expected for the equivalent circuit from which Figure 2 was obtained, and this result is independent of trap states. At low frequencies, however, the real impedance increased dramatically due to the charging and discharging of trap sites caused by the superimposed alternating current. The impedance value at 10^{-4} s^{-1} ($2\pi \times 10^{-4}$ Hz) was nine orders of magnitude higher than the corresponding limit at high frequency.

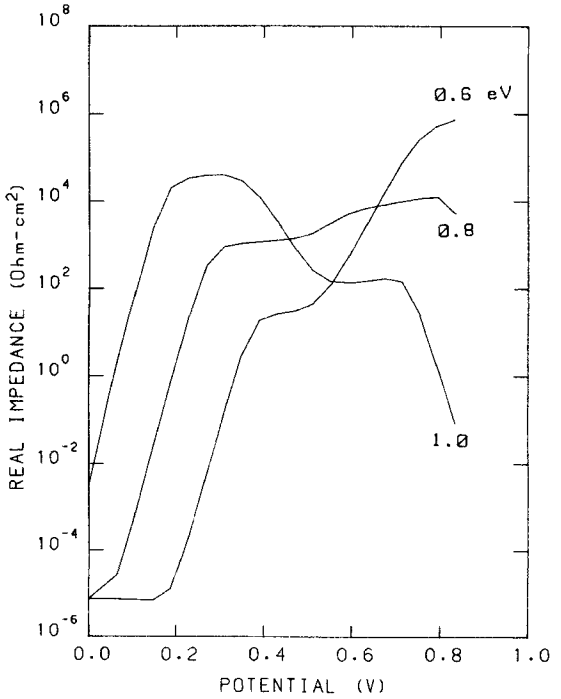

Figure 4. Real part of impedance as a function of applied potential (referenced to flat-band potential) with trap energy as a parameter for a nonuniform trap distribution.
Applied frequency, 10^{-4} s^{-1}

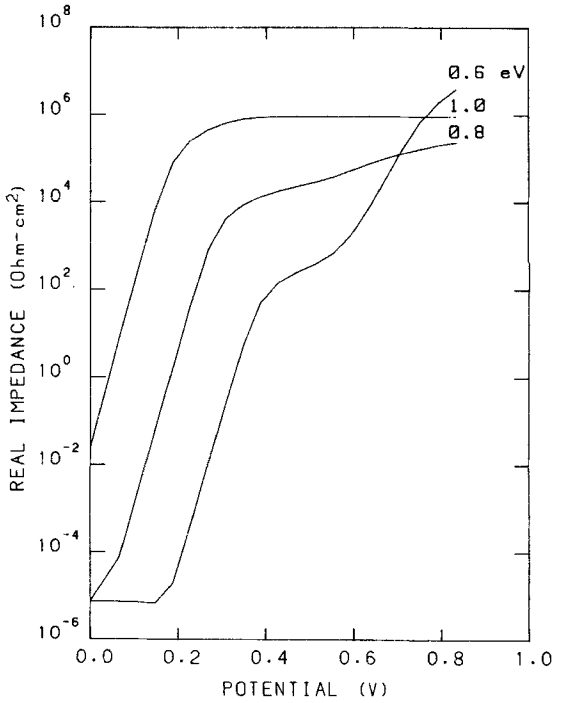

Figure 5. Real part of impedance as a function of applied potential (referenced to flat-band potential) with trap energy as a parameter for a uniform trap distribution.
Applied frequency, 10^{-4} s^{-1}

The value of the real part of the impedance at low frequencies is sensitive to the energy, distribution, and concentration of trap states. For example, the real part of the impedance at 10^{-4} s^{-1} is presented as a function of potential in Figure 4 with trap energy as a parameter. A value of 0.8 eV referenced to the valence band energy was chosen to emulate that of chromium, an important deep-level acceptor species in GaAs. These plots show maxima that are not apparent with a uniform distribution of traps, Figure 5. The sensitivity of the real part of the impedance to even very low trap concentrations is shown in Figure 6 for a uniform distribution of chromium. In the absence of trap sites, the real part of the impedance follows the high-frequency asymptote.

The calculated dependence on the near-surface distribution of electronic states is consistent with the experimental observations of Nagasubramanian et al. (1983), who report that the real part of the impedance goes through a maximum when the potential is increased from the flat-band potential. This maximum was not observed when surface treatment was said to prevent formation of surface states. The resistivity of the real part of the impedance to surface states was greatest at the lowest frequencies studied (25 Hz). Their results were obained with TiO_2 in acetonitrile solutions, rather than with GaAs; however, these calculations should apply to their system with appropriate changes of transport and kinetic parameters.

The equivalent circuit shown in Figure 7 was used to correlate the data with frequency-independent components. Dare-Edwards et al. (1983) presented a mathematical development based on an analytic solution of the transport equations that lead

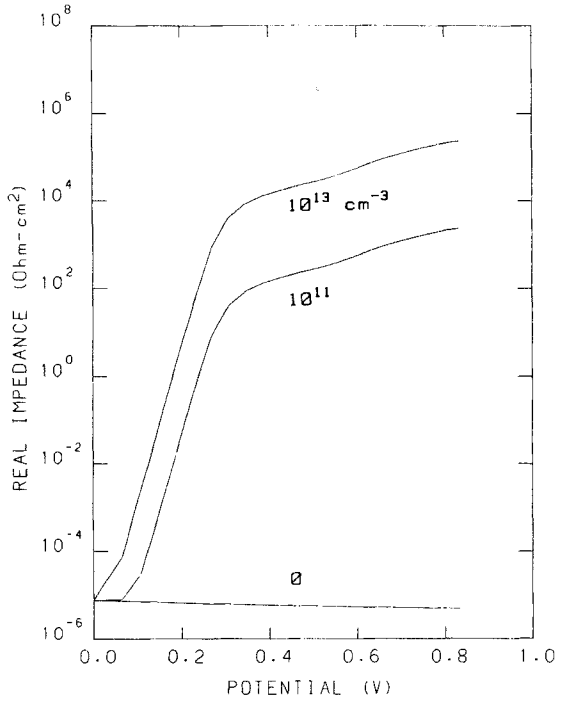

Figure 6. Real part of impedance as a function of applied potential (referenced to flat-band potential) with trap site density as a parameter for a uniform distribution of sites with energy 0.8 eV referenced to valence band energy.

Applied frequency, 10^{-4} s^{-1}

to the same equivalent circuit, again based on the effect of surface states and neglecting the effect of bulk states. This equivalent circuit provides results that match those calculated by our model, which does not treat surface states but does treat bulk deep-level electronic states. The real and imaginary components of impedance based on the equivalent circuit given in Figure 7 are

$$Z_r = R_2 + \frac{C_1^2 R_1}{(C_1 + C_2)^2 + \omega^2 (C_1 C_2 R_1)^2} \tag{9a}$$

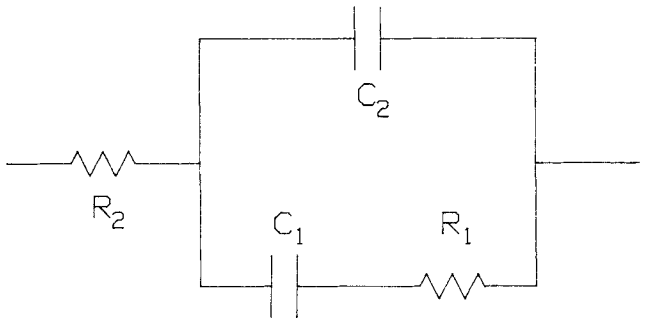

Figure 7. Equivalent circuit that gives the same results as numerical calculations including the effect of mid-bandgap electronic states.

Values of circuit components are independent of frequency but are functions of potential

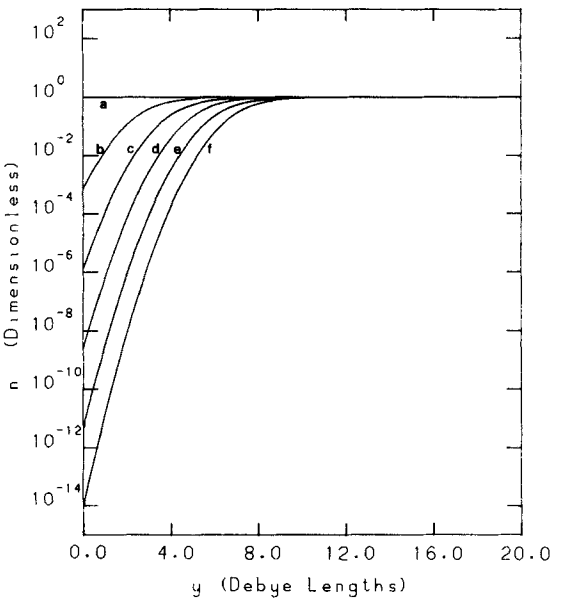

Figure 8. Concentration distribution for electrons with applied potential (referenced to flat-band potential) as a parameter.

a. 0 V d. 0.51 V
b. 0.19 V e. 0.67 V
c. 0.35 V f. 0.84 V

and

$$Z_j = -\frac{C_1 + C_2 + \omega^2 C_1^2 C_2 R_1^2}{\omega (C_1 + C_2)^2 + \omega^3 (C_1 C_2 R_1)^2} \tag{9b}$$

respectively. The capacitive component is insensitive to trap states because, at the low concentrations used here, the capacity C_1 (space-charge capacity contribution associated with mid-bandgap electronic states) is negligible. Thus the imaginary component of the impedance is given by $Z_j = -1/\omega C_2$. In contrast, the real part of the impedance is a function of R_1 and C_1 at low frequencies, but is independent of these terms as ω becomes large.

An interesting result of this work is that the same equivalent circuit matches both the results of our model that treats the effect of bulk states and the model of Dare-Edwards et al. (1983), which treats the effect of surface states. One should be able to use the potential dependence of component values (or, more easily, the real part of the impedance) to determine for a given experiment whether bulk or surface states are responsible for this behavior. The calculated low-frequency real impedance exhibits a maximum as a function of potential for a distribution of electronic states that is highly localized near the surface and does not exhibit a maximum for uniform distribution; see Figures 4 and 5, respectively. The power of applied potential as a probe to resolve spatial distributions can be seen from the calculated distributions of steady and perturbation variables. For example, the steady state distribution of electron concentration is given in Figure 8 with applied potential as a parameter. Corresponding values of the real part of the perturbation variable $\tilde{n}_r$ are shown in Figure 9. This variable shows maxima at roughly the spatial position where the steady state electron concentration is 0.5. Electrons must be strongly perturbed in order to fill

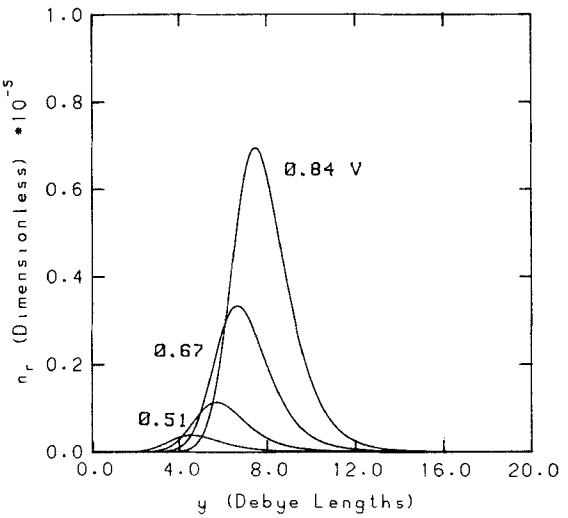

Figure 9. Concentration distribution for real component electron concentration $\tilde{n}_r$ with applied potential (referenced to flat-band potential) as a parameter.

states that are completely empty or to leave states that are completely filled at steady state. These states, therefore, do not contribute to the real impedance of semiconductors, whereas partially filled states do have a significant contribution. Since the applied potential shifts the spatial location in the semiconductor where states are partially filled, resolution of nonuniform distributions of electronic states within the bandgap is possible.

Conclusions

The imaginary component of the impedance is sensitive to doping level and the flat-band potential, but is insensitive to the influence of bulk electronic states within the band gap if the concentration of these states is significantly less than the doping level. The real component, however, is sensitive to bulk states in the low-frequency limit, and this sensitivity may be used to discern the trap energy, concentration, and distribution of these states. These effects are seen in the low-frequency limit, and the frequency at which these are seen to depend on the rate constants for recombination.

The work presented here suggests that a comparison of model calculations with measured impedance may lead to a nondestructive test from which trap concentration, distribution, and identity may be inferred. The experimental setup that would be used for this test is essentially the same as that commonly used to measure doping level distributions from changes in the slope of Mott-Schottky plot as functions of potential. More work is needed to determine whether the coupling of this mathematical model with experimental measurement of impedance could be used to characterize bulk properties of semiconductors; however, the experimental evidence of the type of behavior predicted by the model has been reported and has been attributed to deep-level surface states.

Acknowledgment

This material is based upon work supported in part by the National Science Foundation under Grant No. EET-8617057. During the course of this work, D. B. Bonham was supported by a fellowship from Texaco.

Notation

c_A = total concentration of ionized and neutral deep-level acceptor species, M
c_{A^-} = concentration of ionized deep-level acceptor species, M
c_i = concentration of species i, M
C_1 = space-charge capacitance associated with deep-level acceptor states obtained from an equivalent electrical circuit, Figure 7 and Eq. 9, F/m^2
C_2 = space-charge capacitance associated with shallow-level dopant species obtained from an equivalent electrical circuit, Figure 7 and Eq. 9, F/m^2
D_i = diffusivity of species i, m^2/s
E_c = conduction band edge energy, eV
E_g = band gap energy $E_c - E_v$, eV
E_t = trap state energy, eV
E_v = valence band edge energy, eV
E_{jk} = equilibrium constant for forward reaction j and backward reaction k; see Figure 1 for indices associated with specific reaction pathways
F = Faraday's constant, 96,487 C/equiv.
g = degeneracy of acceptor states; $g = 4$ for electron-acceptor states, $g = 2$ for electron-donor states (Sze, 1969).
i = current density, A/m^2
$j = \sqrt{-1}$
k = Boltzman's constant, 8.62×10^{-5} eV/K
k_j = rate constant for reaction j
n = electron concentration, M
n_i = intrinsic carrier concentration, M
N_a = ionized acceptor concentration; includes both shallow- and deep-level states, M
N_c = effective density of conduction-band states, M
N_d = ionized donor concentration; includes both shallow- and deep-level states, M
N_v = effective density of valence-band states, M
N_{yi} = molar flux of species i, mol/m^2 · s
p = hole concentration, M
q_{sc} = magnitude of charge held in space-charge region of semiconductor, C
R = universal gas constant, 8.314 J/K · mol
R_i = volumetric rate of generation of species i, mol/m^3 · s
R_1 = semiconductor resistance associated with deep-level acceptor states obtained from an equivalent electrical circuit, Figure 7 and Eq. 9, Ω/m^2
R_2 = semiconductor resistance associated with shallow-level dopant species obtained from an equivalent electrical circuit, Figure 7 and Eq. 9, Ω/m^2
t = time, s
T = absolute temperature, K
u_i = mobility of species i, m^2/V · s
$\bar{x}$ = steady state symbol for variable x where x can be c_{A^-}, n, p, or Φ
$\tilde{x}_r$ = real component of perturbation in variable x where x can be c_{A^-}, n, p, or Φ
$\tilde{x}_j$ = imaginary component of perturbation in variable x where x can be c_{A^-}, n, p, or Φ
y = distance from interface, m
z_i = charge number for species i
Z = complex impedance, Ωm^2

Greek letters

ϵ_{sc} = semiconductor permittivity, Farad/m
λ = Debye length, m
Φ = electrostatic potential, V
$\Delta\tilde{\Phi}$ = difference in real or imaginary components of perturbation variable for potential between ohmic contact and ideally polarizable interface, V
ω = frequency, 1/s

Literature Cited

Allongue, P., and H. Cachet, "Band-Edge Shift and Surface Charges at Illuminated n-GaAs/Aqueous Electrolyte Junctions," *J. Electrochem. Soc.*, **132**, 45 (1985).

Butler, M. A., and D. S. Ginley, "Chemically Induced Interface States in Photoelectrochemical Cells," *Appl. Phys. Lett.*, **42**, 582 (1983).

Cheng, C. Y., and D.-T. Chin, "Mass Transfer in AC Electrolysis. I: Theoretical Analysis Using a Film Model for Sinusoidal Current on a Rotating Hemispherical Electrode," *AIChE J.*, **30,** 757 (1984a).
———, "Mass Transfer in AC Electrolysis. II: Experimental Study with Sinusoidal Current," *AIChE J.*, **30,** 765 (1984b).
———, "Mass Transfer in AC Electrolysis. III: Study of Triangular and Square-Wave Current on a Rotating Electrode," *AIChE J.*, **31,** 1372 (1985).
Dare-Edwards, M. P., A. Hamnett, and P. R. Trevellick, "Alternating-Current Techniques in Semiconductor Electrochemistry," *Chem. Soc., Faraday Trans. 1,* **79,** 2111 (1983).
DeClerck, G., R Van Overstraeten, and G. Broux, "Measurement of Low Densities of Surface States at the Si-SiO_2-Interface," *Solid-State Electron.*, **16,** 1451 (1973).
Fahrenbruch, A. L., and R. H. Bube, *Fundamentals of Solar Cells: Photovoltaic Solar Energy Conversion,* Academic Press, New York, 55–67 (1983).
Gärtner, W. W., "Depletion-Layer Photoeffects in Semiconductors," *Phys. Rev.*, **116,** 84 (1959).
Ghandhi, S. K., *VLSI Fabrication Principles, Silicon and Gallium Arsenide,* Wiley, New York, 30 (1983).
Ghosh, A. K., F. G. Wakim, and R. R. Addiss, Jr., "Photoelectronic Processes in Rutile," *Phys. Rev.*, **184,** 979 (1969).
Grove, A. S., *Physics and Technology of Semiconductor Devices,* Wiley, New York, 117–148 (1967).
Haak, R., and D. Tench, "Electrochemical Photocapacitance Spectroscopy Method for Characterization of Deep-Level and Interface States in Semiconductor Materials," *J. Electrochem. Soc.*, **131,** 275 (1984a).
———, "Cadmium Selenide Interface States Studied by Electrochemical Photocapacitance Spectroscopy," *J. Electrochem. Soc.*, **131,** 1442 (1984b).
Haak, R., C. Ogden, and D. Tench, "Electrochemical Photocapacitance Spectroscopy: A New Method for Characterization of Deep Levels in Semiconductors," *J. Electrochem. Soc.*, **129,** 891 (1982).
Haak, R., D. Tench, and M. Russak, "Charge Transfer via Interface States at Polycrystalline Cadmium Selenide Electrodes," *J. Electrochem. Soc.*, **131,** 2709 (1984).
Heller, A., K.-C. Chang, and B. Miller, "Photocurrent Spectroscopy of Semiconductor Electrodes in Liquid Junction Solar Cells," *J. Am. Chem. Soc.*, **100,** 684 (1978).
Kamieniecki, Emil, "Surface Photovoltage Measured Capacitance: Application to a Semiconductor/Electrolyte System," *J. Appl. Phys.*, **54,** 6481 (1983).
Kelly, J. J., and R. Memming, "The Influence of Surface Recombination and Trapping on the Cathodic Photocurrent at p-Type III-V Electrodes," *J. Electrochem. Soc.*, **129,** 730 (1982).
Kobayashi, K., M. Takata, and S. Okamoto, "AC Impedance Theory for Surface States at a Semiconductor-Liquid Junction," *J. Electroanal. Chem.*, **185,** 47 (1985).
Laser, D., and A. J. Bard, "Semiconductor Electrodes. VII: Digital Simulation of Charge Injection and the Establishment of the Space-Charge Region in the Absence and Presence of Surface States," *J. Electrochem. Soc.*, **123,** 1828 (1976a).
———, "Semiconductor Electrodes. VIII: Digital Simulation of Open-Circuit Photopotentials," *J. Electrochem. Soc.*, **123,** 1833 (1976b).
Li, J., and L. M. Peter, "Surface Recombination at Semiconductor Electrodes. III: Steady-State and Intensity Modulated Photocurrent Response," *J. Electroanal. Chem.*, **193,** 27 (1985).
McCann, J. F., and D. Hanneman, "Recombination Effects on Current-Voltage Characteristics of Illuminated Surface Barrier Cells," *J. Electrochem. Soc.*, **129,** 1134 (1982).
McDonald, J. R., "Theory of AC Space-Charge Polarization Effects in Photoconductors, Semiconductors and Electrolytes," *Phys. Rev.*, **92,** 4 (1953).
———, "Static Space-Charge and Capacitance of a Single Blocking Electrode," *J. Chem. Phys.*, **29,** 1346 (1958).
Morisaki, H., and K. Yazawa, "Electroluminescence at the n-TiO_2/Electrolyte Interface," *Appl. Phys. Lett.*, **33,** 1013 (1978).
Nagasubramanian, G., B. L. Wheeler, and A. J. Bard, "Semiconductor Electrodes. XLIX: Evidence for Fermi Level Pinning and Surface-State Distributions from Impedance Measurements in Acetonitrile Solutions with Various Redox Couples," *J. Electrochem. Soc.*, **130,** 1680 (1983).
Nakato, Y., A. Tsumura, and H. Tsubomura, "Electro- and Photo-Luminescence Spectra in Various n-Type Semiconductors in Relation with Anodic Reaction Intermediates," *Chem. Phys. Lett.*, **85,** 387 (1982).
Newman, J., "Numerical Solution of Coupled Ordinary Differential Equations," *Ind. Eng. Chem. Fundam.*, **7,** 514 (1968).
———, *Electrochemical Systems,* Prentice-Hall, Englewood Cliffs, NJ, 173, 217–237 (1973).
Nicollian, E. H., and A. Groetzberger, "The Si-SiO_2 Interface: Electrical Properties as Determined by the Metal-Insulator-Silicon Technique," *Bell Sys. Tech. J.*, **46,** 1055 (1967).
Orazem, M. E., "A Mathematical Model for the Photoelectrochemical Etching of Semiconductors," *Electrochemical Engineering Applications,* R. E. White, R. F. Savinell, A. Schneider, eds., *AIChE Symp. Ser.,* New York, 25 (1987).
Orazem, M. E., and J. Newman, "Mathematical Modeling of Liquid-Junction Photovoltaic Cells. I: Governing Equations," *J. Electrochem. Soc.*, **131,** 2569 (1984a).
———, "Mathematical Modeling of Liquid-Junction Photovoltaic Cells. II: Effect of System Parameters on Current-Potential Curves," *J. Electrochem. Soc.*, **131,** 2574 (1984b).
———, "Photoelectrochemical Devices for Solar Energy Conversion," *Modern Aspects of Electrochemistry,* v. 18, R. E. White, J. O'M. Bockris, B. E. Conway, eds., Plenum, New York, 61 (1986).
Pettinger, B., H.-R. Schoppel, and H. Gerischer, "Electroluminescence at Semiconductor Electrodes Caused by Hole Injection from Electrolytes, *Ber. Bunsenges. Phys. Chem.*, **180,** 849 (1976).
Schwartz, R. J., J. L. Gray, and M. S. Lundstrom, *Report on High Intensity Solar Cells,* Sandia Nat. Lab. Rept. SAND84-7002 (1985).
Sze, S. M., *Physics of Semiconductor Devices,* Wiley, New York, 11–76 (1969).
Tomkiewicz, M., "The Potential Distribution at the TiO_2 Aqueous Electrolyte Interface," *J. Electrochem. Soc.*, **126,** 1505 (1979).
Tribollet, B., and J. Newman, "Impedance Model for a Concentrated Solution: Application to the Electrodissolution of Copper in Chloride Solutions," *J. Electrochem. Soc.*, **131,** 2780 (1984).
Wheeler, B. L., G. Nagasubramanian, and A. J. Bard, "Semiconductor Electrodes. LVII: Differential Photocurrent and Second Harmonic Techniques for *in situ* Monitoring of Surface States on n-$MoSe_2$ in Aqueous Solutions," *J. Electrochem. Soc.*, **131,** 2289 (1984).

Manuscript received June 14, 1987 and revision received Oct. 19, 1987.